Finite-range-scaling analysis of metastability in an Ising model with long-range interactions

Bryan M. Gorman and Per Arne Rikvold
Supercomputer Computations Research Institute, Department of Physics, and Center for Materials Research and Technology, Florida State University, Tallahassee, Florida 32306

M. A. Novotny
Supercomputer Computations Research Institute, Florida State University, Tallahassee, Florida 32306-4052
(Received 1 December 1993)

We apply both a scalar field theory and a recently developed transfer-matrix method to study the stationary properties of metastability in a two-state model with weak, long-range interactions: the $N \times \infty$ quasi-one-dimensional Ising model. Using the field theory, we find the analytic continuation $\tilde{f}$ of the free energy across the first-order transition, assuming that the system escapes the metastable state by the nucleation of noninteracting droplets. We find that corrections to the field dependence are substantial, and, by solving the Euler-Lagrange equation for the model numerically, we have verified the form of the free-energy cost of nucleation, including the first correction. In the transfer-matrix method, we associate with the subdominant eigenvectors of the transfer matrix a complex-valued "constrained" free-energy density f_α computed directly from the matrix. For the eigenvector with an associated magnetization most strongly opposed to the applied magnetic field, f_α exhibits finite-range scaling behavior in agreement with $\tilde{f}$ over a wide range of temperatures and fields, extending nearly to the classical spinodal. Some implications of these results for numerical studies of metastability are discussed.

PACS number(s): 64.60.My, 64.60.Qb, 02.70.Rw, 03.50.Kk

I. INTRODUCTION

Determining the stationary properties of metastable states from the standpoint of statistical mechanics has been the topic of many studies over the last three decades. (For reviews, see, e.g., Refs. [1,2].) Some early treatments of this problem have shown that traditional methods of equilibrium statistical mechanics in a more generalized form might be applicable to metastable states. In a study of the analytic properties of the free energy at the condensation point, Langer [3] conjectured that the imaginary part of the free energy $\widetilde{F}$ analytically continued from the equilibrium phase across the first-order phase transition may be associated with the decay rate of the metastable phase. A dynamical investigation of thermally activated nucleation [4,5] showed that for a wide class of models, the decay rate Γ may be written as

$$\Gamma = \frac{\beta\kappa}{\pi}|\mathrm{Im}\widetilde{F}|\,, \tag{1}$$

where β is the inverse temperature $1/k_{\mathrm{B}}T$, and κ is a kinetic prefactor that contains all dependence on the dynamics.

Subsequently there have been a number of theoretical and numerical studies of metastable decay. Binder and collaborators [6–8] developed a scaling theory based on a proposed definition of metastable states in terms of a nonequilibrium relaxation function and tested this theory by Monte Carlo simulation on the two-dimensional (2D) Ising model. Schulman and co-workers studied by various methods metastability in the 2D Ising model [9], in the 1D Kac model with algebraically decaying interactions [10], in the Curie-Weiss model [11], and in a dropletlike "urn" model [12]. In addition, Büttiker and Landauer [13,14] studied nucleation in the overdamped 1D sine-Gordon chain, and Klein and Unger [15,16] used a ϕ^3 field theory to study systems with long-range interactions in arbitrary dimensions near the classical spinodal. Other studies of nucleation in short-range systems also exist in the literature, including field-theoretical studies [17–19], series expansions [20–23], and exact diagonalization studies [24]. Each of the above studies supported the validity of Langer's treatment. Recently Gaveau and Schulman [25] have determined a rigorous upper bound for Γ for a larger class of models than that considered by Langer, and have used it not only to explain why Eq. (1) is usually valid, but also to provide an example in which it can give misleading results.

A study of the analytic properties of transfer-matrix eigenvalues led to a conjecture [26] that there is a correspondence between the analytically continued free-energy density $\tilde{f}$ and the analytic continuation of the dominant eigenvalue of the transfer matrix. This conjecture has been supported by subsequent numerical studies [9,27,28] of the 2D Ising model. In a similar study [29] of an Ising model with $N \times \infty$ cylindrical geometry in which the interaction range is linear in the cross section, evidence from the transfer-matrix eigenvalue spectrum was found for the emergence of a classical spinodal in the limit of weak, long-range interactions. In the present work we apply a recently developed "constrained-transfer-matrix" (CTM) method [30–33] to study the properties of the metastable phase of this quasi-one-

dimensional Ising (Q1DI) model. Since the transfer matrix for the $N\times\infty$ Q1DI model has a rank of $N+1$ [29], instead of the typical value of 2^N for short-range Ising systems, it is relatively easy to study large systems by transfer-matrix techniques. Using the CTM method, we obtain a "constrained" free-energy density associated with the metastable phase. Our main focus here will be to relate the finite-size (or equivalently for this model, finite-*range*) scaling behavior of the constrained free energy to the scaling behavior of the analytic continuation of the free energy for an equivalent one-dimensional long-range field-theoretical model. This work represents an extension to metastable states of our recent study [34] of critical equilibrium finite-range scaling in the Q1DI model.

In studies of condensation it is often useful to consider the behavior of long-range models. One reason for this is that long-range models share many of the equilibrium and metastable properties of mean-field models, which are often exactly soluble. In addition, as with equilibrium states near the critical point, the metastable states of these models near the classical spinodal may be studied using a simple field-theoretical Hamiltonian [15,16]. Further, the behavior of many physical systems, such as coherent metal-hydrogen systems [35], superfluid ^{3}He [36], long-chain polymer mixtures [37,38], materials exhibiting elastic phase transitions [39], superconductors [40], and ferroelectrics with long-range strain fields [41,42], indeed are well described by long-range models with suitably chosen order parameters. Many treatments of classical metastability for these models are reported in the literature, using many different approaches: the Fokker-Planck equation [11,43,44], the properties of the nonequilibrium relaxation function [6,44], renormalization group analysis [45], and Monte Carlo simulation [43,44,46,47], in addition to analytic continuation of the free energy [11,15,16]. The approach of the present work is to calculate numerically from the transfer matrix a constrained free-energy density [30,31] associated with the classical metastable state, and to determine its scaling behavior in weak fields away from the critical point, and near the classical spinodal. We demonstrate that this quantity is closely related to the analytically continued free-energy density.

The remainder of this paper is outlined as follows. In Sec. II we derive the Euler-Lagrange equation for the order parameter in the Q1DI model, and we identify the solutions corresponding to the equilibrium and metastable phases, as well as the most likely fluctuation through which a Q1DI system in the metastable phase can decay into the equilibrium phase. In Sec. III we obtain a mapping of the Q1DI model near the classical spinodal to a one-dimensional ϕ^3 field theory. Using both the solution to the Euler-Lagrange equation and the field theory, we perform the analytic continuation of the free energy for the model across the first-order phase transition, obtaining an exact expression for its imaginary part near the classical spinodal. In Sec. IV we give a brief overview of the CTM method, which is based on the notion of "constrained" joint probability densities [30,31], and we show how the symmetries of the Q1DI model [29] are used to simplify the calculation. In Sec. V we verify by numerical integration of the Euler-Lagrange equation the temperature and field dependence of the the free-energy cost of nucleation, including the first field correction. We also present our numerical transfer-matrix results and compare them with finite-range-scaling predictions for $\tilde{f}$ based on the field-theoretical results of Sec. III. In Sec. VI we summarize our conclusions, and we discuss the implications of the results to the applicability of the CTM method to studies of metastability.

II. THE Q1DI MODEL

The quasi-one-dimensional Ising, or Q1DI, model [29] is a one-dimensional chain of L subsystems, or layers, each of which contains N Ising spins $s_{i,n}=\pm1$, where the index $i=1,\ldots,L$ runs over the layers, and the index $n=1,\ldots,N$ runs over the spins in a given layer. Each spin interacts ferromagnetically with each of the $2N$ spins in the adjacent layers with a coupling $J/N>0$ and with the other $N-1$ spins of its own layer with a coupling J'/N. Each spin also interacts with an external magnetic field H. The Hamiltonian is explicitly

$$\mathcal{H} = -\sum_{i=1}^{L}\left(\frac{J}{N}\sum_{n=1}^{N}\sum_{n'=1}^{N} s_{i,n}s_{i+1,n'} + \frac{J'}{N}\sum_{n=1}^{N-1}\sum_{n'=n+1}^{N} s_{i,n}s_{i,n'} + H\sum_{n=1}^{N} s_{i,n}\right), \tag{2}$$

where periodic boundary conditions are imposed, that is, $(\forall i,n)\ s_{L+i,n}=s_{i,n}$. The sums over n and n' in Eq. (2) may be performed directly, so this Hamiltonian may be expressed in terms of a discrete field ϕ of layer magnetization densities $\phi_i=N^{-1}\sum_{n=1}^{N} s_{i,n}$ as

$$\mathcal{H}[\phi] = -N\sum_{i=1}^{L}\left[J\phi_i\phi_{i+1} + \tfrac{1}{2}J'(\phi_i^2 - N^{-1}) + H\phi_i\right]. \tag{3}$$

The partition function may then be written as

$$Z = \sum_{\phi} g[\phi]e^{-\beta\mathcal{H}[\phi]}, \tag{4}$$

where

$$g[\phi] = \prod_{i=1}^{L}\binom{N}{\frac{1}{2}N(1+\phi_i)} \tag{5}$$

denotes the multiplicity of spin configurations giving rise to ϕ. In the limit of large N, the probability density of ϕ is sharply peaked around its maximum, so if we define a free-energy-density functional as

$$\mathcal{F}[\phi] = (NL)^{-1}\left\{\mathcal{H}[\phi] - \beta^{-1}\ln(g[\phi])\right\}, \tag{6}$$

then the free-energy density is

$$f_{\mathrm{Q1DI}} = -(\beta NL)^{-1}\ln Z \approx \min_{\phi}\mathcal{F}[\phi]. \tag{7}$$

Applying Stirling's approximation to Eq. (5), combining the result with Eqs. (3) and (6), and removing constant

terms, we have for the Q1DI model

$$\mathcal{F}[\phi] = \frac{1}{L}\sum_{i=1}^{L}\left[\tfrac{1}{2}J(\phi_{i+1}-\phi_i)^2 + f_{\rm CW}(\phi_i)\right] , \qquad (8)$$

where

$$f_{\rm CW}(\phi_i) = -\tfrac{1}{2}\beta_c^{-1}\phi_i^2 - H\phi_i + \beta^{-1}\left(\frac{1+\phi_i}{2}\ln\frac{1+\phi_i}{2} + \frac{1-\phi_i}{2}\ln\frac{1-\phi_i}{2}\right) \qquad (9)$$

is the free-energy density of a Curie-Weiss ferromagnet with a critical temperature

$$\beta_c^{-1} = 2J + J' . \qquad (10)$$

Corrections to $f_{\rm CW}$ due to finite N will be briefly considered in Sec. VI.

In Ref. [34] we showed, both analytically and numerically, that the critical equilibrium N-scaling relations for the Q1DI model are those of an $N\times\infty$ cylindrical Ising model above its upper critical dimension, which can be obtained from a standard one-dimensional ϕ^4 field theory by a single rescaling of the correlation length. Here we extend our study of the scaling behavior to metastable states, where $\beta>\beta_c$ and $H\neq 0$, by studying the scaling behavior of the analytic continuation of the free energy across the first-order phase transition. To do this, we must first calculate the free-energy density for the equilibrium and metastable phases of the model, as well as the height of the free-energy barrier between them. For large N, we can treat each ϕ_i as a continuous variable. In this case, extremizing $\mathcal{F}[\phi]$ with respect to ϕ in the L cube $[-1,1]^L$, we obtain a system of L coupled nonlinear equations:

$$L\frac{\partial\mathcal{F}}{\partial\phi_i} = -J(\phi_{i+1}-2\phi_i+\phi_{i-1}) + \frac{\partial f_{\rm CW}(\phi_i)}{\partial\phi_i} = 0 . \qquad (11)$$

We can gain some understanding of the solutions to Eq. (11) by expressing the equation in differential form. We define a function $\phi(r)$ to be continuous in a dimensionless longitudinal coordinate r, and we force $\phi(r)=\phi_i$ at integer values $r=i$. By Taylor's theorem, if $i\le r\le i+1$, then $(\phi_{i+1}-\phi_i)^2 = [\nabla\phi(r)]^2 + O(\nabla\phi\nabla^2\phi)$. Therefore, if $\phi(r)$ does not vary too rapidly over the length of the chain, then the free-energy density is well approximated by the Ginzburg-Landau-Wilson form:

$$\mathcal{F}[\phi] = \frac{1}{L}\int_0^L dr\,\left[\tfrac{1}{2}J(\nabla\phi)^2 + f_{\rm CW}(\phi(r))\right] , \qquad (12)$$

which represents an effective interaction range

$$R_N = \sqrt{\beta_c J N} , \qquad (13)$$

as measured in sites. Note, however, that R_N is finite as measured in layers. In the critical region, this mapping to the continuum field theory agrees with the formulation in Ref. [34]. The resulting Euler-Lagrange equation for stationary solutions is the continuous analogue to Eq. (11):

$$L\frac{\delta\mathcal{F}[\phi]}{\delta\phi(r)} = -J\frac{d^2\phi}{dr^2} + \left.\frac{\partial f_{\rm CW}}{\partial\phi}\right|_{\phi(r)} = 0 , \qquad (14)$$

which can be integrated once to give

$$\tfrac{1}{2}J\left(\frac{d\phi}{dr}\right)^2 = f_{\rm CW}(\phi(r)) - C , \qquad (15)$$

where C is a constant.

Equation (14) may be interpreted as the equation of motion for a particle of mass J moving in a potential $-f_{\rm CW}(\phi(r))$, where $\phi(r)$ represents the displacement of the particle at time r. Detailed descriptions of the solution from this point of view can be found in Refs. [3,16]. In determining the solutions, we assume that $\phi(r)$ is continuous. Since $f_{\rm CW}$ is continuous on the interval $[-1,1]$ and continuously differentiable on $(-1,1)$, $\phi(r)$ is twice continuously differentiable on $(-1,1)$. The boundedness of ϕ requires that if the left-hand side of Eq. (15) is nonzero for all r, it must approach zero as $|r|\to\infty$, since ϕ would in that case be monotone, while the nonnegativity of the left-hand side of Eq. (15) requires that $(\forall r)\ f_{\rm CW}(\phi(r))\ge C$. The first condition on the solution is therefore that the range of ϕ is an interval $I\subset[-1,1]$ for which $\inf[f_{\rm CW}(I)]=C$. Further, we must have as a second condition that $f_{\rm CW}(\phi)=C$ at the end points of I. To see this, assume on the contrary that $f_{\rm CW}(\phi')>C$ for one of the end points ϕ'. For some r we would then have $\phi(r)=\phi'$ and $|d\phi/dr|>0$ by Eq. (15), forcing $\phi(r)$ to violate the first condition by taking values outside the interval I.

By varying the constant C we find three types of solutions satisfying the above constraints. These are illustrated in Fig. 1. The first type (I) is a completely uniform solution, in which $d\phi/dr=d^2\phi/dr^2=0$ for all r. By Eq.

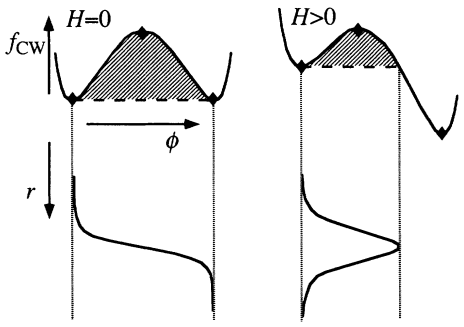

FIG. 1. Schematic diagrams of the solutions to Eq. (14) for the cases of $H=0$ and $H>0$. The solutions are shown together with sketches of the corresponding Curie-Weiss free-energy density $f_{\rm CW}$. The diamonds mark the uniform (type-I) solutions. The dashed horizontal line in each case represents the interval over which the order parameter ranges in the type-II solution. The hashed regions represent the bands of type-III solutions, which oscillate in space between magnetization densities with the same value of $f_{\rm CW}$. Below these sketches of the intervals are sketches in real space of the type-II solutions.

(14), these solutions exist only if the constant value of $\phi(r)$ is an extremum of $f_{\rm CW}$. There can be as many as three solutions of this type, and they are marked on the free-energy sketches in Fig. 1 as diamonds. The second type of solution (II) is a nonuniform "droplet" or "interface" solution, in which one of the end points of I is the locus of a local minimum $\phi_{\rm ms}$ of $f_{\rm CW}$ that is not a unique global minimum. If such a minimum exists, there is only one solution of this type. The vertical lines descending from the free-energy sketches in Fig. 1 mark the end points of the range of $\phi(r)$ for this solution, and sketches of the solution in real space are drawn below. If the type-II solution exists, then a band of solutions of a third type (III) also exists. These solutions are oscillatory in space and are marked on the free-energy sketches in Fig. 1 as hashed regions. They are not considered in the following discussion since the free-energy densities associated with these solutions are the highest of those for the three types.

By considering the solutions of types I and II, we easily identify the equilibrium and metastable states as those with the two lowest values of $\mathcal{F}$. Both are uniform (type-I) solutions, $\phi(r)=\phi_{\rm eq}$ and $\phi(r)=\phi_{\rm ms}$, respectively, and thus by Eq. (11) have $\mathcal{F}[\phi]=f_{\rm CW}(\phi_{\rm eq})$ and $\mathcal{F}[\phi]=f_{\rm CW}(\phi_{\rm ms})$, respectively. The metastable state exists at temperatures and fields for which $f_{\rm CW}$ exhibits two minima. For $\beta>\beta_c$, this is true if $\phi_{\rm ms}$ does not coincide with a point of inflection of $f_{\rm CW}$. The locus of the inflection is given by $\phi=\pm\sqrt{1-\beta_c/\beta}$, so the metastable state exists if $\phi_{\rm ms}^2>1-\beta_c/\beta$. Combining this constraint with Eq. (11) and with the uniformity of ϕ, we obtain the classical (Curie-Weiss) spinodal field H_s [11,44], which defines the limit of metastability:

$$H_s=-\beta_c^{-1}\phi_s+\beta^{-1}\tanh^{-1}\phi_s\ , \tag{16}$$

where

$$\phi_s=-(\mathrm{sgn}H)\sqrt{1-\beta_c/\beta}\ . \tag{17}$$

The solution with the next-lowest value of $\mathcal{F}$ is the type-II solution. This solution represents the fluctuation of lowest free energy through which the metastable phase can decay into the equilibrium phase (for $H\neq0$), or through which a system can pass between two coexisting phases (for $H=0$).

For $0<|H|<|H_s|$, we can estimate the free-energy cost ΔF of this fluctuation by numerically solving the coupled nonlinear equations defined by Eq. (11) for an L-layer system, allowing the magnetization densities to vary continuously. In Sec. V the numerical integration procedure is outlined and its results for ΔF are compared with the analytic result from a field-theoretical Hamiltonian near the spinodal and with our transfer-matrix results.

III. ANALYTIC CONTINUATION OF F

For the Q1DI model with $\beta>\beta_c$, the free energy F in the limit $N\to\infty$ is not everywhere analytic, but rather exhibits a discontinuous first derivative with respect to H at $H=0$. However, if we vary H continuously through $H=0$, an analytic continuation $\tilde{f}$ of the free-energy density across $H=0$ does exist as an analogue of Eq. (7), where the partition function is constrained to configurations that do not allow the system to reach equilibrium. This continuation is the minimum of $\mathcal{F}$ that coincides with $f_{\rm Q1DI}$ at $H=0$, but increases as H departs from zero. When H reaches the spinodal field, the metastable minimum vanishes. At this point the continuation has a branch point and becomes complex as $|H|$ is increased further.

We determine the leading behavior of the analytic continuation of F in the region of the spinodal ($\phi=\phi_s$, $H=H_s$) as follows. Taking the continuum limit used in the preceding section, we write $\phi(r)=\phi_s+v(r)$ and $H=H_s+\lambda$, and we expand Eq. (12) for the free-energy-density functional near the spinodal to third order:

$$\mathcal{F}[T,H,\phi]=\mathcal{F}[T,H_s,\phi_s]+\Delta\mathcal{F}\ , \tag{18}$$

with

$$\begin{aligned}\Delta\mathcal{F}&=\frac{1}{L}\int_0^L dr\left[\tfrac{1}{2}J(\nabla v)^2+\lambda\frac{\partial f_{\rm CW}}{\partial H}\bigg|_{\phi_s}+\lambda v\frac{\partial^2 f_{\rm CW}}{\partial\phi\partial H}\bigg|_{\phi_s}\right.\\&\qquad\left.+\tfrac{1}{6}v^3\frac{\partial^3 f_{\rm CW}}{\partial\phi^3}\bigg|_{\phi_s}+O(v^4)\right]\\&=-\lambda\phi_s+\frac{1}{L}\int_0^L dr\left[\tfrac{1}{2}J(\nabla v)^2\right.\\&\qquad\left.-\lambda v+\tfrac{1}{3}\alpha v^3+O(v^4)\right]\ ,\end{aligned} \tag{19}$$

where we find

$$\alpha=\frac{\beta^{-1}\phi_s}{(1-\phi_s^2)^2}=-(\mathrm{sgn}H)\frac{\beta}{\beta_c^2}\sqrt{1-\frac{\beta_c}{\beta}} \tag{20}$$

using the explicit form of Eq. (9) for $f_{\rm CW}$ and Eq. (17). In Eq. (19) we have shown only the derivatives that are not identically zero. (Since $f_{\rm CW}$ is stationary and has an inflection at $\phi=\phi_s$, the first and second ϕ derivatives are among those not shown.) From the above expansion, the requirement that $\mathcal{F}$ is stationary gives the Euler-Lagrange equation

$$-J\nabla^2 v-\lambda+\alpha v^2+O(v^3)=0\ . \tag{21}$$

Since the critical fluctuation consists of a single droplet, the free-energy cost of the fluctuation is not extensive in L. We take the position of the droplet core to be $r=0$ in the following discussion. Since this fluctuation is local, the solution to Eq. (21) must be asymptotically uniform in the limit $L\to\infty$, that is, $v(r)\to$const as $|r|\to\infty$. From Eq. (21) we thus have asymptotically

$$v\to v_0=(\lambda/\alpha)^{1/2}+O(\lambda) \tag{22}$$

with the sign restriction $\mathrm{sgn}v_0=\mathrm{sgn}\alpha$ if $|H|<|H_s|$. Changing variables to $u(r)=v(r)-v_0$, the Euler-Lagrange equation becomes

$$-J\nabla^2 u+2\alpha v_0 u+\alpha u^2+O(u^3)=0\ . \tag{23}$$

In the limit $|r|\to\infty$ we may neglect terms of $O(u^2)$. We thus obtain

$$u(r) \sim \exp(-r/\xi_r) , \tag{24}$$

where

$$\xi_r = \sqrt{\tfrac{J}{2}}|\alpha\lambda|^{-1/4} + O(\lambda^{1/4}) \tag{25}$$

is the relaxation length of the fluctuation. The power-law dependence on λ of the order parameter v_0 and the length scale ξ_r is indicative of a critical point at the spinodal, as was pointed out previously in Refs. [15,16,45]. We can use the change of variables above to separate the L-extensive part of the integral in Eq. (19):

$$\begin{aligned}\Delta\mathcal{F} &= -\lambda\phi_s + \frac{1}{L}\int_0^L dr[\tfrac{1}{2}J(\nabla u)^2 + \alpha(-\tfrac{2}{3}v_0^3 + v_0u^2 + \tfrac{1}{3}u^3) \\ &\qquad + O(v^4)] \\ &= -\lambda\phi_s - \tfrac{2}{3}\alpha v_0^3 + O(v_0^4) - \frac{1}{L}\int_0^L dr[\tfrac{1}{6}\alpha u^3 \\ &\qquad + O(u^4)] ,\end{aligned} \tag{26}$$

where we have integrated $(\nabla u)^2$ by parts and used Eqs. (22) and (23).

If $|H|>|H_s|$, then v_0 is purely imaginary. For the uniform solutions of the Euler-Lagrange equation, $v=\pm i|v_0|$, $\Delta\mathcal{F}$ has an imaginary part given, to this order of approximation, by the second term in Eq. (26). Combining this with Eq. (22) and noting that v_0^4 is real, we have

$$\mathrm{Im}\tilde{f} = \mathrm{Im}(\Delta\mathcal{F}) = \pm\tfrac{2}{3}|\alpha|^{-1/2}|\lambda|^{3/2} + O(\lambda^{5/2}) . \tag{27}$$

This expression is exactly the result for a Curie-Weiss mean-field model [11,44].

On the other hand, if $|H|<|H_s|$, then $\Delta\mathcal{F}$ is purely real, and the first three terms of Eq. (26) give the contribution of the uniform metastable background, whereas the integral term gives the contribution of the critical droplet. Taking the limit $L\to\infty$, we insert the explicit solution to Eq. (21) [14–16],

$$v_1(r) = v_0\left[1 - 3\,\mathrm{sech}^2(r/2\xi_r)\right] , \tag{28}$$

into the integrand in Eq. (26) to find the free-energy cost ΔF of forming the droplet:

$$\begin{aligned}\Delta F &= \tfrac{48}{5}N\xi_r|\alpha|^{-1/2}|\lambda|^{3/2}[1 + O(\lambda^{1/2})] \\ &= \tfrac{24}{5}N\sqrt{2J}|\alpha|^{-3/4}|\lambda|^{5/4} + O(\lambda^{7/4}) .\end{aligned} \tag{29}$$

The first expression for ΔF in Eq. (29) illustrates the difference in the behavior of the analytically continued free energy between long-range models, for which the length scale for the critical droplet is a characteristic length $\xi_r \ll L$ [15,16], and mean-field models, for which the only length scale for fluctuations is the length L of the entire system. The volume extensivity and field dependence of the mean-field result for ΔF [11,44] can be recovered by replacing ξ_r with L in Eq. (29).

Note that if $|H|<|H_s|$, the analytically continued free energy $\tilde{F}$ is real valued only in the limit of infinite interaction range. However, we are interested in the scaling of the free energy for systems with a long, but finite interaction range. For such systems $\tilde{F}$ is complex, but its imaginary part approaches zero rapidly as $R_N\to\infty$. We can determine the scaling properties of the free energy by expanding the partition function for the system under the constraint that all fluctuations remain subcritical. Following Refs. [3,48], we write

$$Z = Z_0 + Z_1 + Z' , \tag{30}$$

where Z_0 is the contribution from the region of configuration space around the local minimum of $\mathcal{F}$ corresponding to the metastable background, Z_1 is the contribution from the region around the saddle point corresponding to the critical droplet, and Z' represents higher-order terms. The free energy must be extensive in L, so we must also consider contributions of multiple critical droplets. If we assume that Z' has contributions only from multiple identical, noninteracting droplets, then by expanding Z as a series in Z_1/Z_0 we have [48]

$$Z = Z_0\exp(Z_1/Z_0) . \tag{31}$$

For the stationary points of $\mathcal{F}$ identified above as the uniform metastable background v_0 and the critical droplet v_1, we write $v(r) = v_n(r) + \nu(r)$ and expand $\mathcal{F}$ to second order:

$$\mathcal{F}[v] \approx \mathcal{F}[v_n] + \delta^2\mathcal{F} , \tag{32}$$

where

$$\begin{aligned}\delta^2\mathcal{F} &= \frac{1}{L}\int_0^L dr\left[\tfrac{1}{2}J(\nabla\nu)^2 + \tfrac{1}{2}\nu^2\left.\frac{\partial^2 f_{\mathrm{CW}}}{\partial\phi^2}\right|_{\phi_s+v_n}\right] \\ &= \frac{1}{L}\int_0^L dr\left\{\tfrac{1}{2}J(\nabla\nu)^2 + \left[\alpha v_n + O(v_n^2)\right]\nu^2\right\} .\end{aligned} \tag{33}$$

In Eq. (33) we have expanded the second term of the integrand to first order in v_n since the values of $v_n(r)$ are small, and we have again used the fact that f_{CW} has an inflection at $\phi=\phi_s$. We diagonalize the quadratic form by a principal-axis transformation $\nu(r)=\sum_j a_j\nu_j$ to the orthonormal set of eigenmodes of the Schrödinger equation

$$-\tfrac{1}{2}J\nabla^2\nu_j + \left[\alpha v_n + O(v_n^2)\right]\nu_j = \omega_j\nu_j . \tag{34}$$

From Eqs. (32)–(34) the resulting contribution Z_n to the partition function can thus be written as a product of decoupled Gaussian integrals:

$$\begin{aligned}Z_n &= \int dv\exp(-\beta NL\mathcal{F}[v]) \\ &= \exp(-\beta NL\mathcal{F}[v_n])\prod_j\int da_j\exp(-\beta Na_j^2\omega_j) .\end{aligned} \tag{35}$$

Note that although the results that appear later in this section are restricted to the region of the spinodal, Eq.

(35) holds everywhere in the region of metastability. It can easily be seen from this and from Eq. (31) that in this region a Boltzmann weight equal to $e^{-\beta\Delta F}$ appears in the analytically continued free energy.

In order to determine the behavior of the analytically continued free energy in the region of the spinodal, where ΔF is small, we must further determine the eigenvalues of Eq. (34). For n=0 Eq. (34) is a free-particle equation with a potential floor at αv_0, whereas for n=1 it describes a particle in a potential well described by $\alpha v_1(r)$. There are three localized eigenmodes for n=1 [14]. They are

$$\begin{aligned} \nu_0 &\propto \mathrm{sech}^3(r/2\xi_r), \\ \nu_1 &\propto \mathrm{sech}^2(r/2\xi_r)\tanh(r/2\xi_r), \\ \nu_2 &\propto 4\,\mathrm{sech}(r/2\xi_r) - 5\,\mathrm{sech}^3(r/2\xi_r)\ , \end{aligned} \tag{36}$$

for which

$$\begin{aligned} \omega_0 &= -\tfrac{5}{8}J/\xi_r^2 = -\tfrac{5}{4}|\alpha\lambda|^{1/2} + O(\lambda), \\ \omega_1 &= 0 + O(\lambda), \\ \omega_2 &= \tfrac{3}{8}J/\xi_r^2 = \tfrac{3}{4}|\alpha\lambda|^{1/2} + O(\lambda) \end{aligned} \tag{37}$$

are the respective eigenvalues [49]. The first eigenmode ν_0 is the only unstable mode of fluctuation and corresponds to an increasing or decreasing magnetization at the droplet core. The second eigenmode ν_1 is a translational mode, and the third eigenmode ν_2 corresponds to a widening or narrowing of the droplet. All other eigenmodes are unbounded and form a continuous spectrum with $\omega_j \geq \frac{1}{2}J/\xi_r^2$.

We shall consider the contributions of each localized eigenmode individually. For each ω_j>0, the Gaussian integral of Eq. (35) is a well-defined function, $G(\omega_j) = (\pi/\beta N\omega_j)^{1/2}$, but if $\omega_j \leq 0$, as is the case for j=0 and j=1, the Gaussian integral is divergent. We handle each divergence in a different way. For j=0, we analytically continue $G(\omega)$ from the half plane defined by $\mathrm{Re}\omega$>0 to the entire complex plane. The result is purely imaginary and has a sign ambiguity, since the continuation of G has a branch cut on the negative real axis. For j=1, we use the fact that ν_1 is the normalized derivative of v_1 [Eq. (28)] with respect to r. We can thus make a transformation of the integral to one over dr, the Jacobian of which is simply $\|\nabla v_1\|$. The resulting contributions to Z_1 from the localized modes are

$$\begin{aligned} &\pm\frac{i}{2}\sqrt{\frac{\pi}{\beta N|\omega_0|}} \quad (j=0), \\ &\sqrt{\frac{\Delta F}{NJ}}L \quad (j=1), \\ &\sqrt{\frac{\pi}{\beta N\omega_2}} \quad (j=2)\ . \end{aligned} \tag{38}$$

The factor of $\frac{1}{2}$ has been introduced in the j=0 result [50] to account for the fact that the integral inappropriately counts a divergence as one moves toward the metastable minimum [48]. The form of the j=1 result [50] is quite general and follows from a simple virial argument [17,18]. We are then left with the contributions to Z_1/Z_0 from the continuous spectra of eigenmodes. Using a previous calculation of the ratio of the relevant eigenvalue products in Appendix B of Ref. [14], we obtain

$$\frac{\prod_{j=3}^{\infty} G(\omega_j)}{\prod_{j=0}^{\infty} G(\omega_j^0)} = \frac{\sqrt{30J|\omega_0|\omega_2}}{\xi_r}\left(\frac{\beta N}{\pi}\right)^{3/2}, \tag{39}$$

where ω_j^0 denotes an eigenvalue of the free-particle Schrödinger equation. Combining this with Eqs. (31), (35), (38), and (39), we have [50]

$$\begin{aligned} \mathrm{Im}\tilde{f} &= \pm\sqrt{\frac{15}{2\pi\beta}}\frac{(\Delta F)^{1/2}}{N\xi_r}e^{-\beta\Delta F} \\ &= \pm 12(\sqrt{2J}\pi\beta N)^{-1/2}|\alpha|^{-1/8}|\lambda|^{7/8} \\ &\quad\times[1+O(\lambda^{1/2})]e^{-\beta\Delta F}\ . \end{aligned} \tag{40}$$

Assuming that the dynamics of the system is governed by a Fokker-Planck equation, we have from Ref. [5] that the kinetic prefactor $\kappa=\beta\gamma|\omega_0|$, where γ is the fundamental rate of fluctuation. With Eqs. (1), (38), and (40), this gives the nucleation rate density

$$\begin{aligned} \frac{\Gamma}{NL} &= 15\gamma(\sqrt{2J}N)^{-1/2}\left(\frac{\beta}{\pi}\right)^{3/2}|\alpha|^{3/8}|\lambda|^{11/8} \\ &\quad\times[1+O(\lambda^{1/2})]e^{-\beta\Delta F}\ . \end{aligned} \tag{41}$$

As was pointed out earlier, for large N, unless H is extremely close to H_s, the free-energy cost ΔF of surmounting the nucleation barrier is large, so the exponential factor sets the scale for the metastable lifetime. However, for small N, or for $H\approx H_s$, the lifetime is more strongly dependent on the dynamics and on the detailed structure of the saddle point. In Sec. V we will show how the crossover between these two regimes depends on N by deriving the finite-range-scaling properties of $\mathrm{Im}\tilde{f}$. In the same section we will also directly compare numerical results from the transfer-matrix method outlined in the next section with the exponential weight in Eq. (40), where the gap ΔF is determined numerically from Eq. (11).

IV. THE CONSTRAINED-TRANSFER-MATRIX METHOD

Recently one of us [30,31] introduced a transfer-matrix method, based on the concept of "constrained" joint probability densities, to obtain analogues of the free-energy density for constrained states. Preliminary applications [30–32] to the Q1DI model have shown qualitative agreement between the behavior of the free-energy-density analogue associated with the metastable eigenvalue branch of the transfer matrix and the analytically continued free-energy density. In this study we use this constrained-transfer-matrix method with finite-range scaling [34] to obtain more quantitative results for the scaling of the imaginary part of the metastable "con-

strained" free-energy density. In this section we outline the method, and we describe the use of symmetry reductions in its application to the Q1DI model.

The standard transfer-matrix method is usually applied as follows [51]. Starting with a Hamiltonian for an $N\times L$ q-state system that is invariant under translation in the L direction, such as Eq. (2), we write it as a sum of layer Hamiltonians: $\mathcal{H}=\sum_{i=1}^{L}\bar{\mathcal{H}}(x_i,x_{i+1})$. The layer Hamiltonians $\bar{\mathcal{H}}$ are chosen to depend only on the q^{2N} configurations of a pair of adjacent layers and are chosen so that the form of $\bar{\mathcal{H}}$ is independent of the layer index. We then define the $q^N\times q^N$ transfer matrix $\mathbf{T}$ as an operator in the dual space of configurations $|x_i\rangle\equiv|s_{i,1}\rangle\cdots|s_{i,N}\rangle$ of each of the two adjacent layers:

$$\mathbf{T}=\sum_{x,x'}|x\rangle e^{-\beta\bar{\mathcal{H}}(x,x')}\langle x'|\ . \tag{42}$$

The partition function for the L-layer system with periodic boundary conditions is then $Z=\mathrm{Tr}(\mathbf{T}^L)$, which in the limit $L\to\infty$ gives the free-energy density in terms of the largest eigenvalue λ_0 of $\mathbf{T}$ as $f=-(N\beta)^{-1}\ln\lambda_0$. (Here we index eigenvectors $|\alpha\rangle$, $\alpha=0,1,2,\ldots$, in order of decreasing magnitude of their respective eigenvalues: $\lambda_0>|\lambda_1|\geq|\lambda_2|\geq\cdots$.) Since $\mathbf{T}$ is positive, λ_0 is positive and nondegenerate, and the eigenvector $|0\rangle$ can be chosen to have all positive elements by the Perron-Frobenius theorem [52]. The equilibrium state of the system is characterized by the joint and marginal probability densities

$$P_0(x_i,x_{i+k})=\langle 0|x_i\rangle\langle x_i|(\lambda_0^{-1}\mathbf{T})^{|k|}|x_{i+k}\rangle\langle x_{i+k}|0\rangle,$$
$$P_0(x_i)=\langle 0|x_i\rangle\langle x_i|0\rangle\ . \tag{43}$$

In the following discussion we restrict $\mathbf{T}$ to be symmetric. (For the Q1DI model $\mathbf{T}$ is made symmetric by symmetrizing the layer Hamiltonian $\bar{\mathcal{H}}$.) For each eigenvalue λ_α of $\mathbf{T}$ we define a constrained transfer matrix $\mathbf{T}_\alpha$ to commute with $\mathbf{T}$, so that it can be expanded in the eigenvectors $|\alpha'\rangle$ of $\mathbf{T}$:

$$\mathbf{T}_\alpha=\sum_{\alpha'}|\alpha'\rangle\mu_\alpha(\alpha')\langle\alpha'|\ . \tag{44}$$

The "reweighted" eigenvalues μ_α are chosen to produce "constrained" probability densities,

$$P_\alpha(x_i,x_{i+k})=\langle\alpha|x_i\rangle\langle x_i|(\lambda_\alpha^{-1}\mathbf{T}_\alpha)^{|k|}|x_{i+k}\rangle\langle x_{i+k}|\alpha\rangle,$$
$$P_\alpha(x_i)=\langle\alpha|x_i\rangle\langle x_i|\alpha\rangle\ , \tag{45}$$

in analogy with the equilibrium ($\alpha=0$) case. It was pointed out in Refs. [9,27,28] that the constrained marginal probability densities $P_\alpha(x)$, as defined above, can be interpreted as actual probability densities of single-layer configurations in a constrained state. For example, the expectation value $\langle M\rangle_\alpha$ of the layer magnetization density for a constrained state $|\alpha\rangle$ is given by

$$\langle M\rangle_\alpha=\sum_x P_\alpha(x)M(x)\ . \tag{46}$$

In order to ensure that the entire system is characterized by $P_\alpha(x)$, the matrix $\mathbf{T}_\alpha$ must be chosen so that the constrained joint probability densities $P_\alpha(x,x')$ satisfy the following regularity conditions: (i) that $P_\alpha(x)$ can be obtained by summing over the configurations of one layer, $P_\alpha(x)=\sum_{x'}P_\alpha(x,x')$; (ii) that $P_\alpha(x_i,x_{i+k})$ is well defined for $k=0$, $P_\alpha(x_i,x_i')=\delta_{x_i,x_i'}P_\alpha(x_i)$; and (iii) that $P_\alpha(x_i,x_{i+k})$ reflects stochastic independence in the limit $|k|\to\infty$, $\lim_{|k|\to\infty}P_\alpha(x_i,x_{i+k})=P_\alpha(x_i)P_\alpha(x_{i+k})$. For a matrix $\mathbf{T}_\alpha$ chosen to commute with $\mathbf{T}$, these requirements are satisfied if $\mathbf{T}_\alpha$ has the same rank as $\mathbf{T}$, and if its dominant eigenvalue is λ_α. The reweighting scheme used in this work is

$$\mu_\alpha(\alpha')=\begin{cases}\lambda_\alpha^2/\lambda_{\alpha'}, & \lambda_{\alpha'}>\lambda_\alpha\\ \lambda_{\alpha'}, & \lambda_{\alpha'}\leq\lambda_\alpha.\end{cases} \tag{47}$$

This choice ensures that any fluctuation described by $P_{\alpha'}(x)$, with $\alpha'\neq\alpha$, decays away to the $|\alpha\rangle$ eigenstate with a length scale $|\ln(\lambda_\alpha/\lambda_{\alpha'})|^{-1}$. Thus a fluctuation with $\alpha'<\alpha$, which would otherwise grow, is effectively suppressed. We note, however, that the choice of $\mathbf{T}_\alpha$ given by Eqs. (44) and (47), which satisfies the constraints, is not unique. It is easy to see that we recover the original transfer matrix $\mathbf{T}$ when we set $\alpha=0$.

The "constrained" free-energy density f_α is defined by

$$f_\alpha=\langle\bar{\mathcal{H}}\rangle_\alpha-\beta^{-1}S_\alpha\ , \tag{48}$$

where

$$\langle\bar{\mathcal{H}}\rangle_\alpha=\frac{1}{N}\sum_{x_i,x_{i+1}}P_\alpha(x_i,x_{i+1})\bar{\mathcal{H}}(x_i,x_{i+1}) \tag{49}$$

is the expectation value of $\bar{\mathcal{H}}$ with respect to $P_\alpha(x,x')$, and a generalized entropy S_α is defined using $P_\alpha(x,x')$ in analogy with the source entropy of a stationary, ergodic Markov chain (see, e.g., Ref. [53]):

$$S_\alpha=-\frac{1}{N}\sum_{x_i,x_{i+1}}P_\alpha(x_i,x_{i+1})\mathrm{Ln}\langle x_i|\lambda_\alpha^{-1}\mathbf{T}_\alpha|x_{i+1}\rangle\ . \tag{50}$$

The generalized free-energy density may be written in the form

$$f_\alpha=-\frac{\ln|\lambda_\alpha|}{\beta N}+\frac{1}{\beta N}\sum_{x_i,x_{i+1}}P_\alpha(x_i,x_{i+1})\mathrm{Ln}\frac{\langle x_i|\mathbf{T}_\alpha|x_{i+1}\rangle}{\langle x_i|\mathbf{T}_0|x_{i+1}\rangle}\ . \tag{51}$$

The first term is analogous to the equilibrium case, and the second term is complex valued in general. This is because $\mathbf{T}_\alpha$ is not a positive matrix in general. To see this, note that for $|\alpha\rangle$ ($\alpha\neq0$) to be orthogonal to $|0\rangle$, the elements of $|\alpha\rangle$ must be of mixed sign. Since λ_α is the largest eigenvalue of $\mathbf{T}_\alpha$, the largest contribution to $\mathbf{T}_\alpha$ is the projection $|\alpha\rangle\lambda_\alpha\langle\alpha|$, which must contain negative elements. Therefore the argument to the principal value of the logarithm (Ln) may be negative. We define the domain of Lnz to be $|z|>0$, $-\pi<\arg z\leq\pi$, thus choosing the branch cut along the negative real axis. It is easy to see that if $\alpha=0$, the second term of Eq. (51) vanishes, leaving the equilibrium free-energy density.

The above formalism is applicable to any system for which a symmetric transfer matrix can be written. A CTM study of the two-dimensional Ising ferromagnet with nearest-neighbor interactions is reported in Ref. [33], and a similar study of a three-state model with long-range interactions is reported in Ref. [54]. One reason we have chosen to study the Q1DI model is that the Hamiltonian is invariant under any permutation of spins in a given layer, and thus the rank of the transfer matrix for this model is $N+1$ [29], instead of the typical value of 2^N for short-range Ising systems. We use the low rank of the transfer matrix to our advantage by expressing the matrix in a reduced basis. The computer time and memory saved by this reduction allow us to study systems with very large cross sections.

The reduction proceeds as follows. Let X be the 2^N-dimensional vector space in the basis $\{|x_j\rangle\}$ $(j=1,\ldots,2^N)$ of layer configurations, and let G be the group of spin permutations of the layer, which are represented by unitary operators $\mathbf{U}_k{:}X\to X$ $(k\in G)$. This group partitions $\{|x_j\rangle\}$ into $N+1$ equivalence classes $\mathcal{C}_n$ $(n=0,\ldots,N)$, each of which may naturally be associated with a magnetization m_n. This partition induces a decomposition of the configuration space as $X=\bigoplus X_n$, where each X_n is the subspace spanned by the basis vectors $|x_j\rangle\in\mathcal{C}_n$. That $\mathbf{T}$ is G invariant means that $(\forall k\in G)$ $\mathbf{T}\mathbf{U}_k=\mathbf{T}$, which implies the weaker property that $\mathbf{T}$ commutes with every $\mathbf{U}_k$, and thus may be simultaneously diagonalized with any $\mathbf{U}_k$ by a unitary transformation $\mathbf{S}_k\cdot\mathbf{S}_k^{-1}$. Thus if $\mathbf{D_T}$ and $\mathbf{D}_k$ are diagonal matrices containing the eigenvalues of $\mathbf{T}$ and $\mathbf{U}_k$, respectively, then $\mathbf{D_T}\mathbf{D}_k=\mathbf{S}_k\mathbf{T}\mathbf{U}_k\mathbf{S}_k^{-1}=\mathbf{S}_k\mathbf{T}\mathbf{S}_k^{-1}=\mathbf{D_T}$. Since the eigenvalues of $\mathbf{U}_k$ are roots of unity, it follows that for each eigenvalue of $\mathbf{U}_k$ not equal to unity, the corresponding transfer-matrix eigenvalue is zero. Therefore $\mathbf{T}$ has nonzero eigenvalues only in the subspace of X for which the eigenvalues of $\mathbf{U}_k$ are unity for every $k\in G$. This is the $(N+1)$-dimensional G-invariant subspace of X.

We construct a basis in this subspace as follows. For each class $\mathcal{C}_n$, let $|m_n\rangle$ denote the normalized G-invariant vector projecting only into X_n:

$$|m_n\rangle = g_n^{-1/2}\sum_{x_j\in\mathcal{C}_n}|x_j\rangle\ , \tag{52}$$

where $g_n=\binom{N}{n}$ is the number of basis vectors in $\mathcal{C}_n$. Using Eqs. (42) and (52), we rewrite the transfer matrix in this reduced basis as

$$\begin{aligned}\mathbf{T} &= \sum_{n,n'}\sum_{x\in\mathcal{C}_n}\sum_{x'\in\mathcal{C}_{n'}}|x\rangle e^{-\beta\bar{\mathcal{H}}(x,x')}\langle x'| \\ &= \sum_{n,n'}|m_n\rangle(g_ng_{n'})^{1/2}e^{-\beta\bar{\mathcal{H}}(m_n,m_{n'})}\langle m_{n'}|\ .\end{aligned} \tag{53}$$

We can similarly decompose the sums over configurations present in Eqs. (46) and (49)–(51) into sums over the reduced basis vectors [30]. The transfer-matrix results presented in the next section were obtained using this reduced representation.

V. NUMERICAL RESULTS

In this section we present the results of two numerical methods used to study the properties of the metastable phase in the Q1DI model. We numerically integrate the Euler-Lagrange equation, in the discrete form of Eq. (11), to estimate the free-energy cost of nucleation, which we use to verify the field-theoretical results of Sec. III. We also apply the CTM formalism outlined in Sec. IV to the model. We perform finite-range scaling on the constrained free-energy density f_α of Eq. (51), and we compare the results of the two numerical methods and the theoretical predictions of Sec. III.

A. Numerical integration results

To solve Eq. (11) numerically, we represent the field ϕ as an L vector in which each element is allowed to vary continuously. For the numerical solutions presented in this work we have chosen $L=100$. (Doubling L in this case produced no discernible change in the results for the fields and temperatures we studied.) We set the interaction constants $J=1/2$ and $J'=0$, so that $\beta_c=1$, and we obtained numerical results for temperatures in the range $0.1T_c\le T\le 0.8T_c$. Setting $H>0$, we determine the magnetization density $\phi_{\rm core}$ at the core of the droplet by solving $f_{\rm CW}(\phi_{\rm core})=f_{\rm CW}(\phi_{\rm ms})$ under the constraint $\phi_{\rm core}>\phi_{\rm ms}$. We then force the type-II solution by setting $\phi_1=\phi_{\rm core}$, and $\phi_{L/2}=\phi_{\rm ms}$ as boundary conditions. The layers between $L/2$ and L are given by the symmetry imposed by periodic boundary conditions.

The methods chosen to solve Eq. (11) are the well-known shooting and relaxation methods. (See, e.g., Ref. [55].) Taking the explicit form of Eq. (9) for $f_{\rm CW}$, we use Eq. (11) directly to shoot from $i=1$,

$$\phi_{i+1} = -\phi_{i-1} - H/J + (\beta J)^{-1}\tanh^{-1}\phi_i\ , \tag{54}$$

stopping before the solution becomes catastrophic. The remainder of the system is given the value $\phi_{\rm ms}$, and a relaxation method is employed, using a variant of Eq. (54),

$$\phi_i = \tanh\left\{\beta\left[H+\tfrac{1}{2}J(\phi_{i-1}+\phi_{i+1})\right]\right\}\ . \tag{55}$$

The values are then relaxed iteratively in a checkerboard fashion, each layer being adjusted by an increment $\Delta\phi_i$, until $\sum_i|\Delta\phi_i|<10^{-6}$ for one iteration. The free-energy cost ΔF of forming the droplet is then obtained using Eq. (8):

$$\frac{\Delta F}{N} = \sum_{i=1}^{L}\left[\tfrac{1}{4}(\phi_{i+1}-\phi_i)^2 + f_{\rm CW}(\phi_i) - f_{\rm CW}(\phi_{\rm ms})\right]. \tag{56}$$

In Fig. 2 the numerical solutions for various temperatures are shown as functions of $|\lambda|/H_s=(H_s-H)/H_s$ and are compared with the theoretical result for ΔF from Eq. (29). Corrections to the ϕ^3 field theory are seen to be substantial, especially for low temperatures, except for a region very close to the spinodal. We can account for

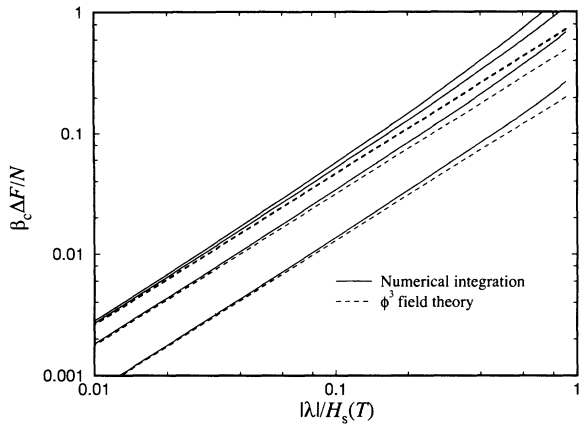

FIG. 2. Estimates for the free-energy cost ΔF of forming the critical droplet in the Q1DI model, shown as a cross-section (N) density and as a function of the H-field deviation from the spinodal, $|\lambda|/H_s = (H_s - H)/H_s$. The solid curves are the results of numerically solving Eq. (11) at temperatures T/T_c=0.2, 0.4, 0.6, and 0.8. The curves corresponding to this order run from top to bottom. The dashed straight lines show the estimates from the ϕ^3 field-theoretical result of Eq. (29) at the same temperatures. These lines appear in the same order, with the two top lines nearly coincident.

this rapid departure of the numerical solutions from the ϕ^3 field theory by considering the leading field-dependent corrections to the cubic potential used in Eq. (19). We can write the first correction to the integrand of Eq. (19) as $\frac{1}{4}\epsilon v^4$, where

$$\epsilon = \frac{1}{6}\frac{\partial^4 f_{\rm CW}}{\partial \phi^4}\bigg|_{\phi_s} = \frac{\beta^2}{\beta_c^3}\left(\frac{4}{3} - \frac{\beta_c}{\beta}\right) . \tag{57}$$

To leading order, the correction to the left-hand side of Eq. (21) is then ϵv^3, and Eq. (26) may be rewritten

$$\Delta\mathcal{F} = -\lambda\phi_s - \tfrac{2}{3}\alpha v_0^3 - \tfrac{3}{4}\epsilon v_0^4 - \frac{1}{L}\int_0^L \left[\tfrac{1}{6}\alpha u^3 + \tfrac{1}{4}\epsilon(2v_0u^3 + u^4)\right] dr . \tag{58}$$

The length scale of the droplet is still given approximately by ξ_r, so performing the integration in the last term introduces a factor of ξ_r. The first correction to ΔF thus has the temperature and field dependence of $\epsilon v_0^4 \xi_r \sim \epsilon|\alpha|^{-9/4}|\lambda|^{7/4}$.

We can verify the presence and form of this correction by studying the behavior of the numerically obtained ΔF as $|\lambda| \to 0$. For a given β, we generate a sequence of field deviations $|\lambda_n| = \lambda_0/n^2$ (not to be confused with the transfer-matrix eigenvalues), where λ_0 is a constant, for an increasing sequence of integers n. We then calculate the free-energy cost of the critical droplet ΔF_n, using the numerical integration procedure outlined above, for a field $H = H_s - \lambda_n$. If we define two sequences $P_n = \Delta F_n/\Delta F$, where ΔF is the analytic result of Eq. (29) at $\lambda = \lambda_n$ with no corrections assumed, and $Q_n = n(P_n - 1)$, then the dominant contributions to ΔF_n should give the following expansions:

$$P_n = 1 + A_1(\beta)n^{-1} + A_2(\beta)n^{-2} + \cdots ,$$
$$Q_n = A_1(\beta) + A_2(\beta)n^{-1} + \cdots , \tag{59}$$

where the amplitudes $A_i(\beta)$ are functions only of β, and in particular, $A_1(\beta) \propto \epsilon|\alpha|^{-3/2}$. For even n, we transform the numerical sequences P_n and Q_n in order to remove the first corrections. The method we use, a variant of Neville-Aitken extrapolation [56], is described in detail in Ref. [34], where it was used to extrapolate with much success finite-size data carrying very substantial corrections. We apply it here to remove $O(n^{-1})$ corrections to P_n and Q_n:

$$P_n' = 2P_n - P_{n/2},$$
$$Q_n' = 2Q_n - Q_{n/2} , \tag{60}$$

which give $P_n' = 1 + O(n^{-2})$ and $Q_n' = A_1(\beta) + O(n^{-2})$. The constancy of the leading terms in P_n and Q_n was verified by calculating estimates W_n^P and W_n^Q to the exponents of n in these terms, which we expect to be zero:

$$W_n^P = (\ln 2)^{-1} \ln(P_n'/P_{n/2}') , \tag{61}$$

and similarly for Q_n, which gives the leading exponent to $O(n^{-2})$. For each temperature, we computed the sequences ΔF_n using $\lambda_0 = 0.5H_s$ and $n = 1, 2, 3, \ldots$. The sequences were terminated when P_n came within 0.5% of unity. The resulting estimates of the $|\lambda|$ exponent ($W_n^P + \frac{5}{4}$) in the leading term lay between 1.249 and 1.251, and the estimates for the $|\lambda|$ exponent in the first correction term ($\frac{1}{2}W_n^Q + \frac{7}{4}$) lay between 1.74 and 1.75, both confirming the field-theoretical predictions of 5/4 and 7/4, respectively [57]. We used the value of P_n' as an estimate for the leading coefficient to P_n. These estimates lay between 0.9998 and 1.0001, confirming Eq. (29) to high accuracy. Dividing the predicted temperature dependence of A_1 from Q_n', we found the resulting coefficient to vary only about 15% over the entire range of temperatures, giving evidence that the predicted temperature dependence of the first correction to ΔF is also as predicted. For $H/H_s \ll 1$, the logarithmic cusp singularity in ΔF predicted in Refs. [3,14] was also observed in our numerical integration results [57]. Since transfer-matrix results were not obtainable at sufficiently low fields, for this work we will not discuss this field region further.

B. Constrained-transfer-matrix results

The CTM method was applied to Q1DI systems of finite cross section N and infinite length, with interaction constants $J = 1/2$ and $J' = 0$, so that $\beta_c = 1$. The temperatures studied using the CTM method were in the range $0.2T_c \le T \le 0.8T_c$, and data at each temperature were collected for fields ranging from $H = 0$ to $H \approx 1.2H_s$. The matrix was tridiagonalized by a Householder reduction, and then diagonalized by an orthogonal-lower-triangular

(QL) decomposition with implicit eigenvalue shifts [55]. The computations were performed in 128-bit precision on a Cray Y-MP 4/32 supercomputer using about 200 CPU hours. Computations were limited mainly by machine precision, since the process described in Sec. IV involves the reweighting and resumming of eigenvalues whose magnitudes range over 30 or more decades. The lower limit on the temperatures studied was due to limited machine precision, whereas the upper limit was due to the extremely large cross sections required to minimize finite-size effects. For most temperatures, systems were studied for N up to the range $100<N<200$, although for the highest temperatures we were able to obtain results for $N\approx500$.

In Fig. 3 typical eigenvalue and layer magnetization spectra of the transfer matrix for the Q1DI model are shown as functions of H. The eigenvalue spectrum is shown on a scale so that its lowest branch is the equilibrium free-energy density of the system. This spectrum can be divided into three regions [29]. The first is a region of low-lying states with positive magnetization. Above this region is a region of alternately polarized states that become nearly degenerate at regular intervals in H. Since all the eigenvectors of the reduced transfer matrix belong to the same symmetry class, the eigenvalue branches are never actually degenerate and therefore do not cross, but rather quickly reverse their direction. In Ref. [29] the gaps between these nearly degenerate eigenvalues were found to approach zero exponentially with N. The quick reversal of the eigenvalue branches can be seen in the near discontinuities in the magnetization branches, in which the values of the magnetizations associated with the two nearly degenerate eigenvalues are effectively traded. This region terminates approximately at the Curie-Weiss spinodal field H_s of Eq. (16). The third region, above the second, consists of eigenvalues that have little polarization. For the results presented here we are concerned with the lowest-lying states of the second region, that is, the lowest-lying states with magnetization opposite the applied magnetic field. These states form a composite branch that agrees well with the values shown for the free-energy density and magnetization of the metastable state for the Curie-Weiss ferromagnet in the thermodynamic limit. This agreement improves as N is increased.

The real and imaginary parts of f_α from the CTM, as computed by Eq. (51), are shown in Fig. 4 for a single system size at fixed temperature. The real part of f_α exhibits a composite branch that is nearly identical to the composite "metastable" branch shown in Fig. 3, and thus is also in good agreement with the known free-energy density of the metastable state. In addition, the corresponding values of $|\mathrm{Im}f_\alpha|$ for this branch are nearly zero except in the region of the spinodal. Figure 5 shows the same branches of $|\mathrm{Im}f_\alpha|$ as Fig. 4 on a logarithmic scale. Note that the values of $|\mathrm{Im}f_\alpha|$ range over more than 30 decades. The structure of the "metastable" branch as a succession of lobes rather than as a smooth function is due to the mixing of nearly degenerate eigenvectors (see Fig. 3). Since we were interested in obtaining values from

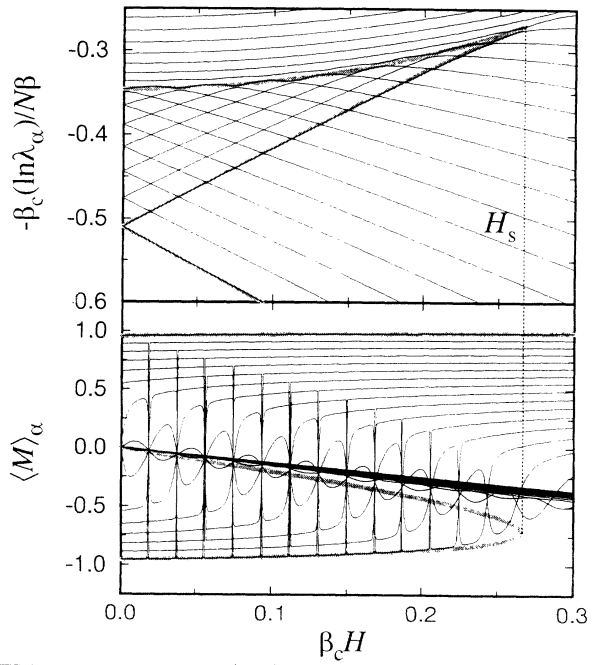

FIG. 3. Eigenvalue (top) and magnetization (bottom) spectra computed from the transfer matrix for a $35\times\infty$ Q1DI system at $T=0.5T_c$ and plotted versus H. The value of the Curie-Weiss spinodal field H_s is marked by the dotted vertical line, and the values of the free-energy density and magnetization for the equilibrium, metastable, and unstable stationary states of the Curie-Weiss ferromagnet are marked by the thick gray lines. Fifteen eigenvalue branches lie above the chosen plotting range, so they are not visible. See Sec. V B for a detailed description.

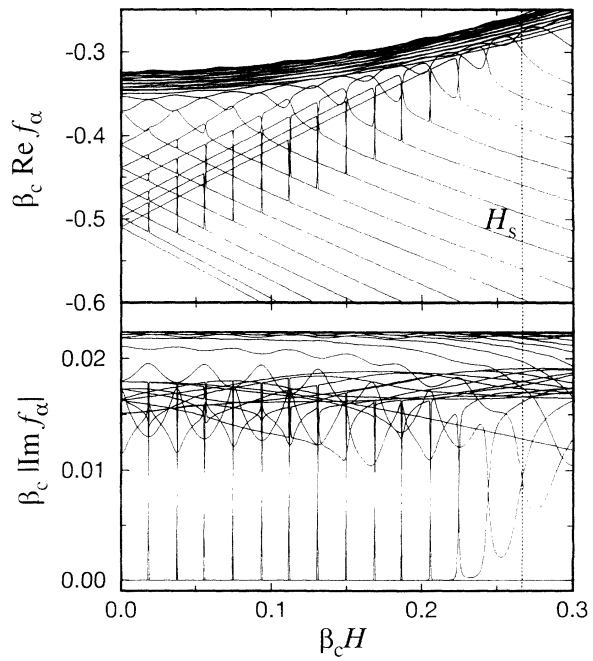

FIG. 4. All branches of $\mathrm{Re}f_\alpha$ (top) and $|\mathrm{Im}f_\alpha|$ (bottom) computed from constrained transfer matrices for a $35\times\infty$ Q1DI system at $T=0.5T_c$ and plotted versus H. The dotted vertical line indicates the spinodal field. The branches of $\mathrm{Re}f_\alpha$ are plotted on the same scale as the eigenvalue branches of Fig. 3, so that the two spectra may be compared directly.

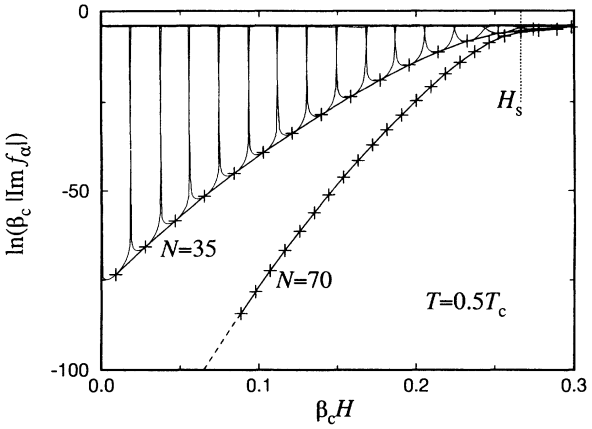

FIG. 5. Branches of $\ln|\mathrm{Im}f_\alpha|$ computed from constrained transfer matrices for a $35\times\infty$ Q1DI system at $T=0.5T_c$ and plotted versus H. The (+) symbols touching the lobes are calculated at fields chosen by the criterion $\lambda_\alpha=(\lambda_{\alpha+1}\lambda_{\alpha-1})^{1/2}$ for the "metastable" eigenvector $|\alpha\rangle$. These points are joined by straight lines. A second set of points, for $N=70$, is shown to illustrate the N-scaling behavior of $\ln|\mathrm{Im}f_\alpha|$. This second set is expected to continue downward at lower fields roughly along the dashed line, but the numerical precision was not sufficient to resolve points in the low-field region. The spinodal field is marked by the dotted vertical line.

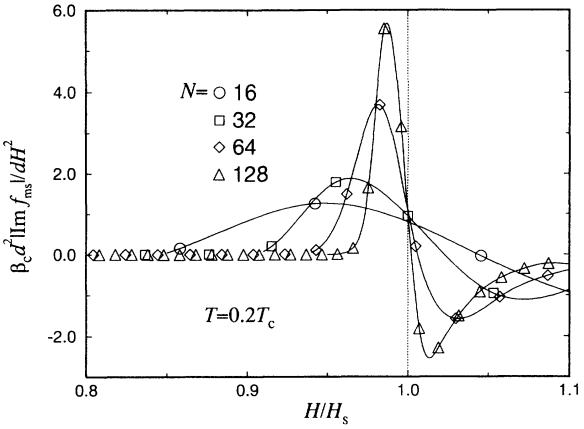

FIG. 6. The second derivative of $|\mathrm{Im}f_\alpha|$ with respect to H for Q1DI systems with various cross sections N at $T=0.2T_c$. The symbols are the results of the midpoint method applied to the points used to define the envelope over the lobes of $|\mathrm{Im}f_\alpha|$. (See Fig. 5.) The lines joining these points are splines serving only as guides to the eye. The dotted vertical line indicates the spinodal field.

branches representing the single "metastable" phase $|\alpha\rangle$, we selected values of H for which $\lambda_\alpha=(\lambda_{\alpha+1}\lambda_{\alpha-1})^{1/2}$, thus ensuring a "safe" distance from the near degeneracies. The resulting points are shown on the figure and together roughly give tangent points for a reasonable envelope for the lobes. We identify this envelope with $\mathrm{Im}f_{\mathrm{ms}}$, the imaginary part of the constrained free-energy density for the metastable state. The envelope for a larger system at the same temperature is also shown. By inspecting the envelopes for many system sizes, we observed roughly an exponential dependence on N well inside the spinodal and a crossover to a slower scaling near the spinodal. The evidence for this scaling behavior will be made clear and quantitative in the next subsection.

The presence of the crossover can be seen clearly in Fig. 6, where the second derivative of $|\mathrm{Im}f_{\mathrm{ms}}|$ with respect to H is plotted versus reduced field H/H_s for a fixed temperature and various values of N. Each derivative was calculated by the midpoint method, using only the "tangent" points chosen as described above. As N increases, a singularity in this derivative develops and pushes closer to the spinodal. Although the value of H_s is temperature dependent, we observed the same behavior in $|\mathrm{Im}f_{\mathrm{ms}}|$ for the entire range of temperatures studied.

C. Finite-range-scaling results

First we turn our attention to the scaling behavior of $|\mathrm{Im}f_{\mathrm{ms}}|$ for fields in the range $0<H<H_s$, and we consider fields far enough from the spinodal that the Boltzmann weight $e^{-\beta\Delta F}$ sets the scale for the metastable lifetime. Since the transfer-matrix data lack the extremely high resolution required to determine the prefactor to this weight, we concentrate on the quantity $\ln|\mathrm{Im}f_{\mathrm{ms}}|$. Assuming a form for $|\mathrm{Im}f_{\mathrm{ms}}|$ as given by Eqs. (29) and (40), we write

$$\ln|\mathrm{Im}f_{\mathrm{ms},N}(T,H)| \sim -\beta N^\sigma \Delta(T,H)\ , \tag{62}$$

where the exponent σ and the function $\Delta(T,H)$ are undetermined.

For each system size N with $N\equiv 0(\mathrm{mod}\ 4)$, we calculate finite-range estimates for σ at fixed T and H assuming that the dominant correction is from the prefactor and is therefore $O(\ln N)$:

$$\sigma_N = (\ln 2)^{-1}\ln\left(\frac{\ln|\mathrm{Im}f_{\mathrm{ms},N}| - \ln|\mathrm{Im}f_{\mathrm{ms},N/2}|}{\ln|\mathrm{Im}f_{\mathrm{ms},N/2}| - \ln|\mathrm{Im}f_{\mathrm{ms},N/4}|}\right)\ , \tag{63}$$

which gives $\sigma_N = \sigma + O(N^{-1})$ [34]. Whereas the values for $\ln|\mathrm{Im}f_{\mathrm{ms},N}|$ in Eq. (63) were taken directly from the tangent points, the values of $\ln|\mathrm{Im}f_{\mathrm{ms}}|$ for smaller systems had to be interpolated to the same field value since both the number and positions of the lobes are N dependent. We performed the interpolation by fitting a quadratic form exactly to the three nearest points. Figure 7 shows σ_N for the largest values of N numerically attainable, plotted versus reduced field for various temperatures. Clearly these estimates are quite consistent with the N dependence ($\sigma=1$) of ΔF given by Eq. (29). Note that as the estimates approach H_s, they drop significantly, indicating the rapidly decreasing importance of the N-dependent exponential factor of $|\mathrm{Im}f_{\mathrm{ms},N}|$ compared to the algebraic prefactor, as was pointed out in Sec. III.

For even N, finite-N estimates for $\Delta(T,H)$ were calculated assuming that $\sigma=1$, and again that the dominant correction is $O(\ln N)$:

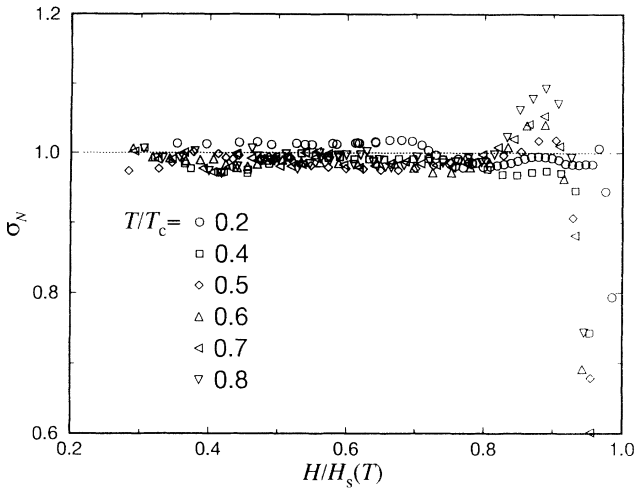

FIG. 7. Finite-N estimates for the exponent σ in Eq. (62), for the largest N attainable, plotted against reduced field H/H_s for various temperatures T. The dotted horizontal line indicates the field-theoretical value (σ=1) over this range.

$$\Delta_N = -\frac{2}{\beta N}(\ln|\mathrm{Im}f_{\mathrm{ms},N}| - \ln|\mathrm{Im}f_{\mathrm{ms},N/2}|) \ . \qquad (64)$$

Values for $\ln|\mathrm{Im}f_{\mathrm{ms},N}|$ were taken as described in the preceding paragraph. Figure 8 shows a typical set of estimates for ΔF. Due to logarithmic corrections, the convergence of naive estimates using Eq. (62) directly, $\Delta(T,H)\approx(\beta N)^{-1}\ln|\mathrm{Im}f_{\mathrm{ms}}|$, is quite slow. Using Eq. (64) gives greatly improved estimates, which agree much better with the free-energy cost of nucleation obtained by numerical integration, and the range of fields over which there is good agreement extends much closer to the spinodal. In addition, these extrapolated estimates show a trend near the spinodal toward the numerical integration result, although the limited accuracy in the interpolations used precluded any further extrapolation.

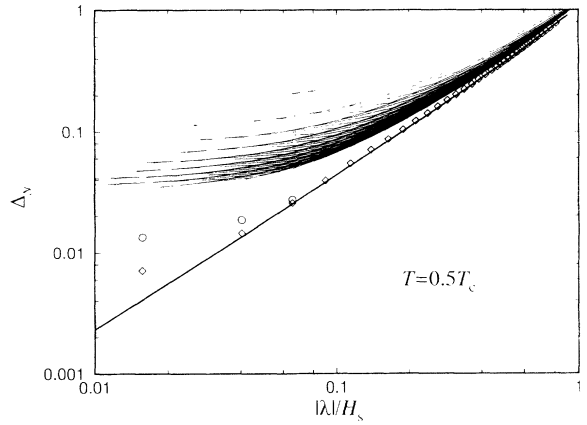

FIG. 8. Finite-N estimates for $\Delta(T,H)$ in Eq. (62) with σ=1 fixed, plotted against $|\lambda|/H_s = (H_s - H)/H_s$ for T=0.5T_c. Each thin line connects the naive estimates one would obtain for a particular N directly from Eq. (62). These estimates decrease in value as N increases. The data points are estimates using Eq. (64). The diamonds are results using the largest N attainable. The circles are results for half of the largest N and are plotted only in the region where finite-size effects are large. The thick line indicates the free-energy cost of forming the numerical "critical droplet" solution of Eq. (11), obtained by numerical integration as described in Sec. V A.

Figure 9 shows Δ_N for the largest values of N numerically attainable, plotted versus reduced field for various temperatures. These are compared with the free-energy cost of nucleation obtained though Eq. (56) by numerically integrating the Euler-Lagrange equation as described in Sec. V A. As can be seen from Figs. 8 and 9, the agreement between the extrapolated CTM estimates and the exact results is impressive. The relative error for these estimates was consistently below 2% over most of the field and temperature range and remained below 5% until the crossover region was entered. By comparing Fig. 9 with Fig. 2, where the free-energy cost of nucleation obtained by numerical integration is shown together with the ϕ^3 field-theoretical results, one sees that the CTM estimates for ΔF faithfully reproduce the higher-order corrections to the ϕ^3 field theory over a wide range of fields and temperatures. This strongly indicates the consistency between the CTM method and the droplet theory of nucleation, at least whenever a substantial free-energy barrier against nucleation exists.

Next we consider the behavior of $|\mathrm{Im}f_{\mathrm{ms}}|$ near the spinodal, where the extrapolated CTM estimates Δ_N lie significantly above the infinite-N free-energy cost ΔF obtained by numerical integration. As discussed in Sec. III, here we must carefully consider the behavior of the prefactor to the Boltzmann weight. Since the mean-field spinodal is a line of critical points in a ϕ^3 field theory, we can apply critical finite-range scaling [34] in this region. By recasting Eqs. (27), (29), and (40) in terms of a scaling variable $\zeta=R_N^{4/5}|\lambda|$, we determine the finite-range scaling relation for $|\mathrm{Im}\tilde{f}|$ to be

$$|\mathrm{Im}\tilde{f}| = R_N^{-6/5}\Phi(\beta,\zeta) \ , \qquad (65)$$

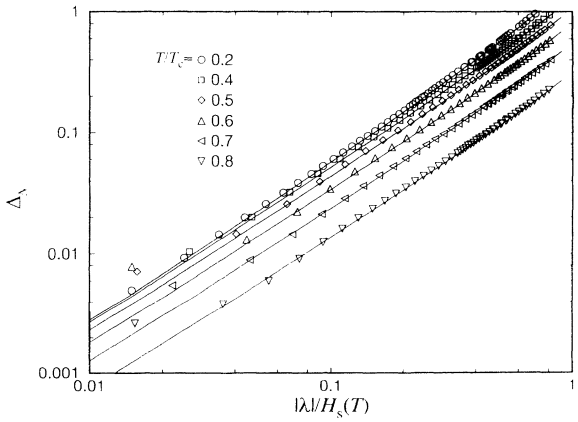

FIG. 9. Finite-N estimates for $\Delta(T,H)$ in Eq. (62) with σ=1 fixed, extrapolated by Eq. (64) for the largest N attainable, and plotted against $|\lambda|/H_s = (H_s - H)/H_s$ for various temperatures T. The lines indicate the free-energy cost of forming the numerical "critical droplet" solution of Eq. (11) at the same temperatures, obtained by numerical integration as described in Sec. V A. Compare with Fig. 2.

where the scaling function Φ depends on the sign of $\lambda = H - H_s$:

$$\Phi(\beta,\zeta) = \begin{cases} 12(\sqrt{2}\pi\beta)^{-1/2}|\alpha|^{-1/8}\zeta^{7/8}\exp\left(-\frac{24}{5}\sqrt{2}\beta|\alpha|^{-3/4}\zeta^{5/4}\right), & |H| < |H_s| \\ \frac{2}{3}|\alpha|^{-1/2}\zeta^{3/2}, & |H| > |H_s| \,. \end{cases} \tag{66}$$

Note that as $\zeta \to 0$ from either direction, Φ goes to zero, with a cusp singularity at $|H| = |H_s|^-$. This singular scaling function cannot be reproduced for finite N. We therefore expect that the finite-N CTM estimates for $|\mathrm{Im}f_{\mathrm{ms}}|$ near H_s should be dominated by corrections to scaling. Indeed, the transfer-matrix results for $|\mathrm{Im}f_{\mathrm{ms}}|$ only showed qualitative agreement with the field theory for $H \approx H_s$. Power-law scaling was found at H_s, but the exponent of R_N varied between roughly -0.8 at low temperatures and -1 at high temperatures, in significant disagreement with Eq. (65), and large fluctuations in the data precluded the use of extrapolation techniques. In addition, the values of the scaling functions calculated from $|\mathrm{Im}f_{\mathrm{ms}}|$ were consistently greater than those of the theoretical scaling functions, varying from a factor of roughly 2 at low temperatures to 5 at high temperatures. Several possible explanations for these results will be considered in the next section.

VI. DISCUSSION

In this work we have applied a scalar field theory and the recently developed constrained-transfer-matrix method to the study of metastability in the ferromagnetic quasi-one-dimensional Ising model, a two-state model with weak, long-range interactions. By solving the Euler-Lagrange equation associated with the Ginzburg-Landau-Wilson Hamiltonian for the model, we have identified the equilibrium and metastable states as spatially uniform configurations with the order parameter taking the Curie-Weiss mean-field values, and we have identified the critical fluctuation through which the metastable state decays. By computing the free-energy cost of the critical fluctuation numerically, we were able to calculate the "Boltzmann weight" that appears in the analytic continuation of the free energy across the first-order phase transition for the entire region of metastability. Except in the region of the classical spinodal, this weight gives the dominant time scale for decay of the metastable state. In the region of the spinodal we have mapped the Hamiltonian to a ϕ^3 field theory to obtain an expression for the analytically continued free energy with no undetermined parameters. Assuming the applicability of the Fokker-Planck equation to the dynamics, we have thus also obtained an exact expression for the decay rate of the metastable state for this model near the classical spinodal. In performing the analytic continuation of the free energy, we have found that its corrections are quite substantial, leading to large differences in, for example, the free-energy cost of nucleation as one moves away from the spinodal toward the first-order transition. Numerical solution of the Euler-Lagrange equation strongly supports the field-theoretical result for the free-energy cost of nucleation, including the first correction term.

We have outlined a method by which a complex analogue of the free energy for a constrained system is obtained directly from the transfer matrix for the unconstrained system. Extensive symmetry reductions have enabled us to collect transfer-matrix data for systems with very large cross sections, and hence very large interaction ranges. We found that the real part of the constrained free-energy density associated with the metastable phase, $\mathrm{Re}f_{\mathrm{ms}}$, rapidly approaches the free-energy density of the metastable phase as $N \to \infty$. The associated imaginary part $|\mathrm{Im}f_{\mathrm{ms}}|$ is extremely small, showing exponential dependence on the interaction range over most of the region of metastability and a crossover to power-law scaling near the classical spinodal. We found strong evidence for this crossover in the behavior of the second field derivative of $|\mathrm{Im}f_{\mathrm{ms}}|$. Using numerical extrapolation techniques, we have demonstrated that over a wide range of fields and temperatures within the region of metastability, the complex "constrained" free-energy density obtained by this method agrees very well with the behavior of the analytically continued free-energy density. The estimated free-energy cost of the critical droplet was found to lie within 2% of the value obtained by solving the Euler-Lagrange equation numerically. In fact, for low temperatures and for fields sufficiently far from the spinodal, the transfer-matrix data were found to agree with the numerical solution much more closely than the analytic field-theoretical results.

However, we found that the constrained free-energy density, as defined by Eq. (51), using the reweighting scheme defined in Eq. (47), does not show consistent finite-range scaling at the spinodal. There are several possible explanations for this result. If we consider the possibility that finite-size corrections to the free-energy cost ΔF of nucleation are affecting the exponents in the prefactor of $|\mathrm{Im}\tilde{f}|$, then those corrections must be $O(\ln N)$ [57]. (This rules out, for example, the effect of relaxing Stirling's approximation, which was used to derive Eq. (8), since it gives only a correction of order unity.) Another possibility is that the effects of eigenvector mixing are too strong in this region to obtain reasonable estimates for $|\mathrm{Im}f_{\mathrm{ms}}|$. In addition, for finite cross sections N, the value of the spinodal may not be entirely real, so that a dominant contribution to $|\mathrm{Im}f_{\mathrm{ms}}|$ emerges from the CTM data due to finite-size rounding. If f_{ms} does represent the analytic continuation of the free-energy density, then it is possible that the eigenvalues are being reweighted incorrectly in this region, allowing unwanted or unphysical fluctuations. These and other possibilities will be explored in further work.

The CTM method clearly shows promise in the characterization of metastable phases. As a nonperturbative method, it treats all possible fluctuations in a single calculation, and hence does not require any particular assumptions about the detailed structure of the partition

function. Since it automatically identifies the fluctuations that are important to nucleation, the CTM method has potential applications to the study of metastability in, for example, disordered systems, in which critical fluctuations are difficult to characterize. The usefulness of this method has been demonstrated in a study of the 2D Ising ferromagnet [33], in which excellent quantitative agreement was found between field-theoretical and CTM estimates of the surface free energy and the shape of the critical droplets, as well as consistency with Monte Carlo estimates of the metastable lifetime [58,59]. Furthermore, in a three-state model with weak, long-range interactions [54], $|\mathrm{Im}f_{\mathrm{ms}}|$ appears to remain consistent with the metastable lifetime, even under conditions of competing metastable states, where it has been argued [25] that the analytic continuation of the free energy may no longer be a valid measure of the lifetime. A Monte Carlo study of metastability in the Q1DI model, using recently developed techniques, is in progress, and a further investigation of the connection between the dynamics of metastable states and the transfer matrix is planned.

ACKNOWLEDGMENTS

We would like to thank T. Fiig and C. C. A. Günther for useful discussions. This work was supported in part by Florida State University through the Supercomputer Computations Research Institute (Department of Energy Contract No. DE-FC05-85ER25000), through the Center for Materials Research and Technology, and through Cray Y-MP supercomputer time, and by National Science Foundation Grant No. DMR-9013107.

[1] J. D. Gunton, M. San Miguel, and P. S. Sahni, in *Phase Transitions and Critical Phenomena*, edited by C. Domb and J. L. Lebowitz (Academic, New York, 1983), Vol. 8.
[2] K. Binder, Rep. Prog. Phys. **50**, 783 (1987).
[3] J. S. Langer, Ann. Phys. (N.Y.) **41**, 108 (1967).
[4] J. S. Langer, Phys. Rev. Lett. **21**, 973 (1968).
[5] J. S. Langer, Ann. Phys. (N.Y.) **54**, 258 (1969).
[6] K. Binder and E. Stoll, Phys. Rev. Lett. **31**, 47 (1973).
[7] K. Binder, Phys. Rev. B **8**, 3423 (1973).
[8] K. Binder and H. Müller-Krumbhaar, Phys. Rev. B **9**, 2328 (1974).
[9] R. J. McCraw and L. S. Schulman, J. Stat. Phys. **18**, 293 (1978).
[10] R. J. McCraw, Phys. Lett. **75A**, 379 (1980).
[11] C. M. Newman and L. S. Schulman, J. Stat. Phys. **23**, 131 (1980).
[12] G. Roepstorff and L. S. Schulman, J. Stat. Phys. **34**, 35 (1984).
[13] M. Büttiker and R. Landauer, Phys. Rev. Lett. **43**, 1453 (1979).
[14] M. Büttiker and R. Landauer, Phys. Rev. A **23**, 1397 (1981).
[15] W. Klein and C. Unger, Phys. Rev. B **28**, 445 (1983).
[16] C. Unger and W. Klein, Phys. Rev. B **29**, 2698 (1984).
[17] C. G. Callan and S. Coleman, Phys. Rev. D **16**, 1762 (1977).
[18] N. J. Günther, D. A. Nicole, and D. J. Wallace, J. Phys. A **13**, 1755 (1980).
[19] W. N. Cottingham, D. Kalafatis, and R. Vinh Mau, Phys. Rev. B **48**, 6788 (1993).
[20] R. J. Baxter and I. G. Enting, J. Stat. Phys. **21**, 103 (1979).
[21] G. A. Baker, Jr. and D. Kim, J. Phys. A **13**, L103 (1980).
[22] M. J. Lowe and D. J. Wallace, J. Phys. A **13**, L381 (1980).
[23] I. G. Enting and R. J. Baxter, J. Phys. A **13**, 3723 (1980).
[24] C. J. Hamer, J. Phys. A **16**, 1247 (1983).
[25] B. Gaveau and L. S. Schulman, Lett. Math. Phys. **18**, 201 (1989).
[26] C. M. Newman and L. S. Schulman, J. Math. Phys. **18**, 23 (1977).
[27] V. Privman and L. S. Schulman, J. Phys. A **15**, L231 (1982).
[28] V. Privman and L. S. Schulman, J. Stat. Phys. **31**, 205 (1982).
[29] M. A. Novotny, W. Klein, and P. A. Rikvold, Phys. Rev. B **33**, 7729 (1986).
[30] P. A. Rikvold, Prog. Theor. Phys. Suppl. **99**, 95 (1989).
[31] P. A. Rikvold, Phys. Scr. **T38**, 36 (1991).
[32] P. A. Rikvold, B. M. Gorman, and M. A. Novotny, in *Slow Dynamics in Condensed Matter*, edited by K. Kawasaki, M. Tokuyama, and T. Kawakatsu, AIP Conf. Proc. No. 256 (AIP, New York, 1992), p. 549.
[33] C. C. A. Günther, P. A. Rikvold, and M. A. Novotny, Phys. Rev. Lett. **71**, 3898 (1993).
[34] P. A. Rikvold, B. M. Gorman, and M. A. Novotny, Phys. Rev. E **47**, 1474 (1993).
[35] H. Wagner and H. Horner, Adv. Phys. **23**, 587 (1974).
[36] A. J. Leggett, Rev. Mod. Phys. **47**, 331 (1975).
[37] P. G. de Gennes, *Scaling Concepts in Polymer Physics* (Cornell University Press, Ithaca, 1979).
[38] K. Binder, Phys. Rev. A **29**, 341 (1984).
[39] R. A. Cowley, Adv. Phys. **29**, 1 (1980).
[40] J. R. Schrieffer, *Theory of Superconductivity* (Addison-Wesley, New York, 1983).
[41] P. B. Littlewood and P. Chandra, Phys. Rev. Lett. **57**, 2415 (1986).
[42] P. Chandra, Phys. Rev. A **39**, 3672 (1989).
[43] R. B. Griffiths, C.-Y. Wang, and J. S. Langer, Phys. Rev. **149**, 301 (1966).
[44] W. Paul, D. W. Heermann, and K. Binder, J. Phys. A **22**, 3325 (1989).
[45] J. D. Gunton and M. C. Yalabik, Phys. Rev. B **18**, 6199 (1978).
[46] T. S. Ray and W. Klein, J. Stat. Phys. **61**, 891 (1990).
[47] T. S. Ray, J. Stat. Phys. **62**, 463 (1991).
[48] L. S. Schulman, in *Techniques and Applications of Path Integration* (Wiley, New York, 1981), Chap. 29.
[49] The expression for ν_1 was misprinted in Eq. (A2) of Ref. [14].
[50] The results of Ref. [16] should be corrected as follows:

(1) the exponent $1/4$ in Eq. (4.8) should be $-1/4$; (2) the exponent $3d/8$ in Eq. (4.11) should be $d(6-d)/8$; and consequently (3) the exponent $(1/2+5d/8)$ in Eq. (4.16) should be $d(1-d/8)$.

[51] C. Domb, Adv. Phys. **9**, 149 (1960).
[52] M. Marcus and H. Minc, *A Survey of Matrix Theory and Matrix Inequalities* (Dover, New York, 1964), p. 124.
[53] R. E. Blahut, *Principles and Practice of Information Theory* (Addison-Wesley, Reading, MA, 1987), pp. 61–64.
[54] T. Fiig, B. M. Gorman, P. A. Rikvold, and M. A. Novotny, FSU-SCRI Report No. 93-160 (1993) (unpublished).
[55] W. H. Press, S. A. Teukolsky, W. T. Vetterling, and B. P. Flannery, *Numerical Recipes* (Cambridge University Press, New York, 1992).
[56] A. J. Guttmann, in *Phase Transitions and Critical Phenomena*, edited by C. Domb and J. L. Lebowitz (Academic, New York, 1990), Vol. 13.
[57] B. M. Gorman (unpublished).
[58] P. A. Rikvold, H. Tomita, S. Miyashita, and S. W. Sides, FSU-SCRI Report No. 94-11 (1994) (unpublished).
[59] C. C. A. Günther, P. A. Rikvold, and M. A. Novotny (unpublished).